Computation of the Voltage-Driven Flux-MMF Diagram for Saturated PM Brushless Motors

TJE Miller, M. Popescu, C. Cossar, M.I. McGilp
SPEED Laboratory, University of Glasgow
Glasgow G12 8LT, U.K.
speedlab.co.uk

***Abstract*—The flux-MMF diagram or "energy conversion loop" is a powerful tool for computing the average torque of saturated permanent-magnet brushless motors, especially when the assumptions underlying classical *dq* theory are violated, as they often are in modern practice. Efficient finite-element computation of the flux-MMF diagram is possible when the motor current is known *a priori*; but in high-speed operation the current-regulator can lose control of the current waveform and the computation becomes "voltage-driven" rather than "current-driven". This paper describes an efficient method for solving the voltage-driven problem together with experimental validation on a small 2-pole brushless interior-magnet motor. The paper also discusses the general conditions when this method is appropriate, and compares it with alternative approaches.**

Keywords — Permanent-magnet brushless motors, torque calculation, finite-element method, simulation

LIST OF SYMBOLS

i,v,ψ	instantaneous current, voltage, and flux-linkage
p	the operator d/dt; or number of pole-pairs
θ	Rotor angular position, rad
L,R,X	Inductance, resistance and reactance
T	Torque, N-m
[]	an array; or value at previous time-step
Δt	integration time-step, s
ω	speed in electrical rad/s
d,q	(subscripts) direct and quadrature axes

I. INTRODUCTION

Brushless permanent-magnet motors are established in a wide range of applications including hybrid vehicles, servo motors, high-efficiency pumping applications and others, while new applications are emerging as a result of their high efficiency, low noise, and controllability, [1,5,10,12]. It is well known that when the magnets are embedded inside the rotor iron, as in the "interior permanent-magnet motor" (IPM), calculations based on classical *dq* theory can be unreliable, mainly because of the variation of parameters due to saturation.

For example X_q in such machines can vary by at least 700% between no-load and full-load, while cross-saturation influences the *d*-axis parameters in a complex manner [1,2,3,4,6]. The difficulties are increased by the use of fractional-slot windings with small numbers of slots/pole (even less than 1), non-circular laminations, and other departures from the ideal machine, so that neither the EMF waveform nor the variation of inductance with rotor position is sinusoidal.

Most previous analyses rely on the classical *dq* model [1-4], and although they allow for cross-saturation effects they restrict themselves to steady-state operation and ignore the effect of rotor position on the *dq*-axis parameters.

As long as the current waveform is known *a priori*, these problems can be overcome in an efficient computation in which the finite-element method is used to determine one cycle of the flux-linkage waveform, which is then plotted against the current waveform to establish a "loop" whose area gives the average electromagnetic torque. This loop diagram is known as the "flux-MMF diagram" or "i-psi loop" or "energy conversion loop", [7]. Bearing in mind that finite-element formulations are fundamentally always "current-driven", the computation is efficient because of the foreknowledge of the current waveform, so that a series of current values can be used as inputs to the finite-element process. This method does not necessarily rely on *dq* theory.

At higher speeds it is normal for the current-regulator to lose control of the current waveform, and ultimately at the highest speeds the drive may operate in six-step mode. In this case the applied *voltage* waveform is known but the *current* waveform is not. Similarly if the machine is generating into a rectifier, the applied voltage at the machine terminals is known or calculable, whereas the current waveform is unknown.

The accuracy of the finite-element method is very desirable in design work, but the problem is how to get quick results, especially in solving the "voltage-driven" problem. Certain finite-element programs can incorporate differential electric-circuit equations in their solvers, but the solution time is a serious problem because it must run out over many cycles until a steady-state is achieved. Some finite-element programs can be coupled to general-purpose system simulation software, [8]. When such general-purpose tools are used, the setup time may be an additional issue. The objective here is to develop a special-purpose method which is specifically designed for rapid computation, and to throw some light on the actual need for voltage-driven finite-element solutions.

II. THEORY

The problem to be solved

The basic problem is to solve the voltage equations of the machine and its drive. For a three-phase machine the voltage equations of the individual phases are:

$$v_a = Ri_a + p\psi_a;\ v_b = Ri_b + p\psi_b;\ v_c = Ri_c + p\psi_c. \quad (1)$$

It is also necessary to know the *magnetization curves*: i.e., the relationship between the flux-linkages ψ and the currents i:

$$\psi_a = \psi_a(i_a,i_b,i_c);\ \psi_b = \psi_b(i_a,i_b,i_c);\ \psi_c = \psi_c(i_a,i_b,i_c). \quad (2)$$

When a simulation program is used to solve eqns. (1), the voltages are known and the currents are unknown. A "time-stepping" solution proceeds by integrating eqns. (1) step-by-step, and from the new flux-linkages at the end of each time-step the currents must be obtained by inverting eqns. (2), ready for the next time-step. Sometimes eqns. (2) are expressed in the form

$$[\psi] = [L(\theta,i_a,i_b,i_c)][i] \quad (3)$$

so that the necessary inversion is a simple matrix operation. Unfortunately, in all but the simplest cases, the self and mutual inductances in the $[L]$ matrix are complicated functions of rotor position θ. When magnetic saturation occurs, they are also functions of current, and then their definition and computation can become ambiguous and obscure. Sometimes eqns. (3) are substituted in eqns. (1) *ab initio*, making currents $[i]$ the state variables instead of flux-linkages $[\psi]$. Since current varies much more rapidly than flux-linkage, it becomes necessary to use a much smaller time-step and the solution becomes much slower.

The finite-element method is fundamentally a method of *evaluating* eqns. (2). Known phase currents i_a, i_b, i_c are expressed as current-density in slot regions, and the unknown flux-linkages ψ_a, ψ_b, ψ_c are computed from line integrals of vector potential along the winding conductors. If the current *waveform* is given , the finite-element method can be used to compute the flux-linkage *waveforms* which can be differentiated with respect to time ($p\psi$) and substituted in eqns. (1) to predict the voltage that would be necessary to achieve the assumed current waveforms. This somewhat "back-to-front" process only works with known current waveforms, but it is quick. Rather than providing a full "voltage-driven" solution, it gives a quick "current-driven" solution together with an indication of the required drive voltage.

Limitations of classical theory

The classical theory of the synchronous machine is based on the *dq* transformation, usually in the form attributed to Park [9]. In the ideal case, it eliminates the rotor position θ from the $[L]$ matrix, producing an immense simplification. For 3-wire connections it reduces the number of currents from 3 to 2, and likewise for the voltages and flux-linkages.

In its classical form this theory rests on two assumptions: (*a*) the windings are sinusoidally distributed around the stator periphery, giving rise to a sinusoidal induced voltage and sinusoidal variation of self- and mutual inductance with rotor position; and (*b*) the magnetic circuit is linear.

If phasors are to be used to describe steady-state operation, it must also be assumed (*c*) that all currents and voltages have sinusoidal time-waveforms. In modern practice *all three* of these assumptions are often violated to some degree, in some cases to such an extent that the classical model gives seriously misleading results.

In spite of these limitations it is still desirable to work in *dq* axes, which are synchronous and fixed to the rotor. This is the natural reference frame for the synchronous machine. Even under non-ideal conditions its simplifying properties are valuable. The *dq* transformation is described in [9] and [12]:

$$\begin{aligned}\psi_d &= \frac{2}{3}[\psi_a\cos\theta+\psi_b\cos(\theta-2\pi/3)+\psi_c\cos(\theta+2\pi/3)];\\ \psi_q &= -\frac{2}{3}[\psi_a\sin\theta+\psi_b\sin(\theta-2\pi/3)+\psi_c\sin(\theta+2\pi/3)].\end{aligned} \quad (4)$$

The same transformation is used for currents and voltages. When it is substituted in eqns. (1), the voltage equations

$$\begin{aligned} v_d &= Ri_d + p\psi_d - \omega\psi_q\\ v_q &= Ri_q + p\psi_q + \omega\psi_d\end{aligned} \quad (5)$$

are obtained. The zero-sequence component is omitted if the machine has no neutral connection.

The transformation is valid even when the idealizations (*a*-*c*) are not satisfied. In that case it is merely a mathematical mapping; eqns. (5) do not inherently require magnetic linearity or sinusoidal winding distributions.

Digital simulation of the machine performance requires the step-by-step integration of eqns. (5). For example, by Euler's method the *d*-axis equation becomes

$$\begin{aligned}\psi_d &= \int(v_d - Ri_d+\omega\psi_q)\,dt\\ &\approx (v_d - Ri_d+\omega\psi_q)\,\Delta t + [\psi_d],\end{aligned} \quad (6)$$

and similarly for the *q*-axis, where $[\psi_d]$ means the value of ψ_d at the previous time-step. At each new time-step, the currents i_d and i_q must be updated from the new flux-linkages, using the magnetization curves.

Mathematical form of the magnetization curves

In the classical synchronous machine with sine-distributed windings and no saturation, these relationships are simple straight lines:

$$\psi_d = \Psi_M + L_d i_d; \quad \text{and} \quad \psi_q = L_q i_q, \quad (7)$$

where L_d and L_q are the synchronous inductances and Ψ_M is a constant flux-linkage produced by the magnet or the field-winding, depending on the type of machine. It is trivial to invert eqns. (7) at each time-step. In the classical case the *d* and *q* axes are uncoupled and the magnetization curves (7) are independent of rotor position θ.

In the *general* case the windings may not be sine-distributed and the magnetic circuit may be saturable. The magnetization curves then have the general form

$$\psi_d = \psi_d(i_d,i_q,\theta) \quad \text{and} \quad \psi_q = \psi_q(i_d,i_q,\theta). \quad (8)$$

The magnetization curves in this form can be obtained by transformation from finite-element evaluations of eqns. (2). In general ψ_d is a function not only of i_d but also of i_q (cross-coupling) and even of θ, and likewise ψ_q is a function of i_d and θ as well as i_q. The functional relationships (8) require a vast number of finite-element calculations to define them [2], as well as an appropriate interpolating function. They are much more complex than eqns. (7), which have the form

$$\psi_d = \psi_d(i_d) \quad \text{and} \quad \psi_q = \psi_q(i_q), \tag{9}$$

in which there is no cross-coupling and no variation with rotor position, and which are easily inverted even when they are nonlinear. Many authors try to limit the extent of the "saturation model" to this form, implicitly ignoring cross-saturation and any variation with rotor position; (see, for example [1,3,4]).

In eqns. (8) the functional influence of θ is due to winding harmonics and any variation of magnetic permeance as the rotor rotates. The obvious source of such permeance variation is on the *stator*. It includes any grain-orientation in the steel; the presence of notches or holes in the lamination, or chamfers and cut-outs at its outer surface; and the effects of slotting.

Even without these effects, and even with sine-distributed windings, if the magnetic circuit is saturable there remains the possibility of a functional influence of θ, induced by the variation of current as the rotor rotates. In well-designed machines the functional influence of θ in eqns. (8) should be weak, otherwise it would be difficult to produce smooth torque. But it requires good calculations to achieve this. With no θ-variation, the magnetization curves have the form

$$\psi_d = \psi_d(i_d, i_q) \quad \text{and} \quad \psi_q = \psi_q(i_d, i_q). \tag{10}$$

This is the form presented in [2], but only in the form of graphical data with no attempt to provide the interpolating function that is necessary in connection with the time-stepped solution of the voltage equations.

III. Managing the Magnetization Curves

In the process of integrating eqns. (6), we have seen that "new" values of ψ_d and ψ_q are generated at each time-step, and that the currents i_d and i_q must be updated. The integration is computationally fast, and therefore our main concern is with the methods for updating the currents, which can be classified as follows:

(A) If there is no magnetic saturation and the windings are sinusoidally distributed, eqns. (7) can be used. This is by far the fastest method, but obviously it requires reliable values of L_d, L_q and Ψ_M.

(B) Method (A) can be modified by precalculating a current-driven i-ψ loop and adjusting the values of L_d, L_q and Ψ_M to take account of saturation and θ-variation in an average sense over one electrical cycle.

(C) As the time-stepping solution proceeds, the values of L_d, L_q and Ψ_M can be updated by means of a single-point finite-element calculation at each time-step, or after an arbitrary number of time-steps, and used in eqns. (7) to determine the currents at the next time-step.

(D) An entire set of magnetization curves can be precalculated in the form of eqns. (8); or in the simplified form of eqns. (9) (with no cross-saturation or θ-variation) or eqns. (10) (with cross-saturation but no θ-variation). Whatever the form of the magnetization curves, the supposition is that they must be precalculated by finite-elements and expressed in a suitable form for time-stepping simulation. The necessary interpolation of the magnetization curves by a numerical curve-fitting function is not a trivial matter and is likely to introduce additional errors. Moreover, this process implies a separation between the computation of the magnetization curves and their use in the time-stepping simulation, which is very inconvenient from the user's point of view.

(E) As the time-stepping simulation proceeds, at each time-step a series of single-point finite-element solutions can be executed under the control of a Newton-Raphson type algorithm which adjusts the currents i_d and i_q to match the flux-linkages computed by means of the circuit simulation. Assuming that four finite-element solutions are required at each iteration (to provide the necessary elements of the Jacobian), and assuming five iterations per point, this method requires 20 times more finite-element solutions than method (C).

Before illustrating some of these methods and comparing them with measured test data, it is of interest to express their relative speeds. Table I expresses the approximate solution times for the motor described later.

TABLE I INDICATIVE SOLUTION TIMES

Method	Solution time for one electrical cycle
A	5 seconds
B	5 minutes
C	1 hour
D	12 hours (less if mag. curves are re-used)
E	20 hours

For normal design work these times suggest that methods A and B are much to be preferred, especially if their accuracy can be substantiated by intermittent use of method C. Taken together, these methods are perfectly sufficient for the current-driven problem. The results presented later suggest that they may also be sufficient for the voltage-driven problem, in which case methods D and E appear to be quite uneconomic.

The average electromagnetic torque is obtained from the sum of the loop areas enclosed within the i-ψ locus for each phase, and examples are given in Figs. (5,6,7,13), [7]. Method (A) is the only one that permits the separation of permanent-magnet alignment torque and reluctance torque. All the others have the possibility of computing torque also by Maxwell stress.

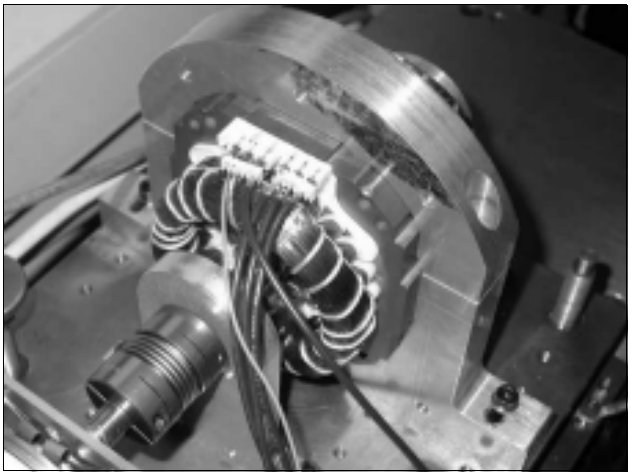

Figure 1. Motor on test stand

IV. Experimental Test

Fig. 1 shows the testing of a small 2-pole brushless IPM motor which is controlled by a PWM inverter (not shown). The motor cross-section is shown in Fig. 2. Each magnet pole comprises three separate NdFeB magnets. The three-phase winding has two pole-groups per phase, each with four coils having turns and coil-pitches of 50/11; 46/9; 40/7 and 30/5 respectively. The rotor diameter is 62 mm and the stack length is 48.6 mm. There is no skew.

Fig. 3 shows the open-circuit EMF waveform of the blue phase at 500 rpm, together with its fundamental and the finite-element-calculated waveform. The measured and calculated fundamentals agree within about 5%. The actual waveform has a considerable ripple component due to the stator slotting combined with the rotor structure with three magnet blocks per pole. Further complications are introduced by the complex outer shape of the stator lamination, and the presence of eight holes in this lamination. None of these details are modelled in the finite-element calculation, which uses the cross-section in Fig. 2. Thus although the windings are reasonably sinusoidally distributed, the permeance harmonics result in considerable ripple in the EMF. There is also an asymmetry in the EMF waveform caused by the squared-off shape of the stator lamination and the non-uniform stator yoke section. This affects the three phases differently according to their positions.

Fig. 4 shows the open-circuit flux-linkage corresponding to Fig. 3, together with the fundamental component. The flux-linkage is computed directly by finite-elements, and differentiated to get the EMF waveform in Fig. 3. The test version of the flux-linkage waveform, however, is obtained in the opposite direction by integrating the EMF in Fig. 3. All mathematical operations on the waveforms are done in software after recording them with a digital recording oscilloscope.

The importance of the open-circuit waveforms is to show the degree to which the motor might appear to be amenable to analysis by dq theory. In spite of the ripple in the EMF, the sinusoidal shape of the flux-linkage in Fig. 4 suggests that good results should be obtained for the average torque.

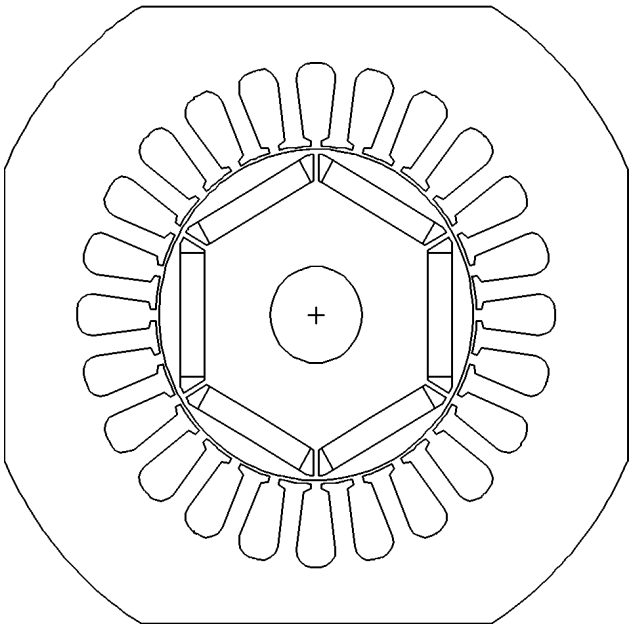

Figure 2. Motor cross-section

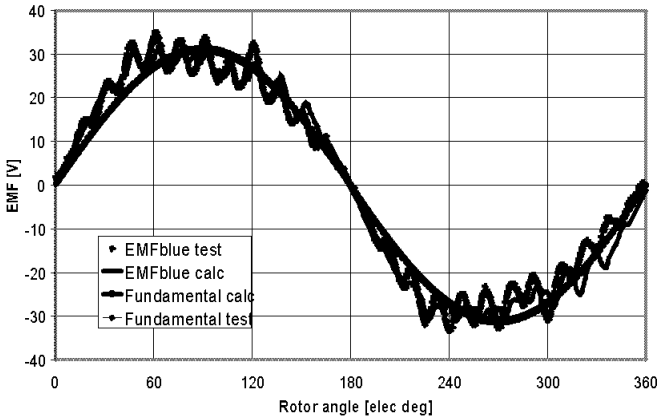

Figure 3. Open-circuit EMF (blue phase)

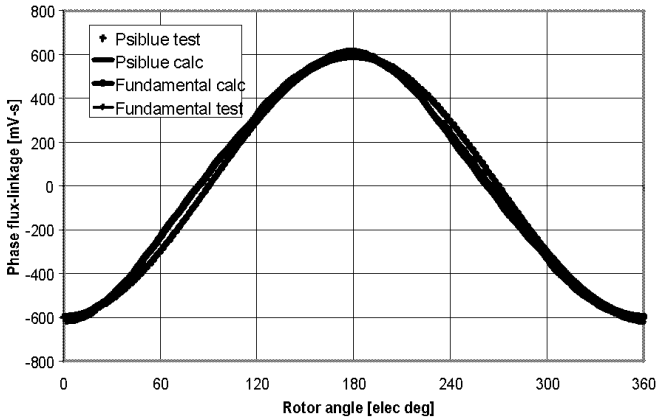

Figure 4. Open-circuit flux-linkage (blue phase)

Note that the flux densities in the teeth and yoke are very high, approaching 1.8 T even in the open-circuit condition, so the machine is highly saturated and becomes more so under load.

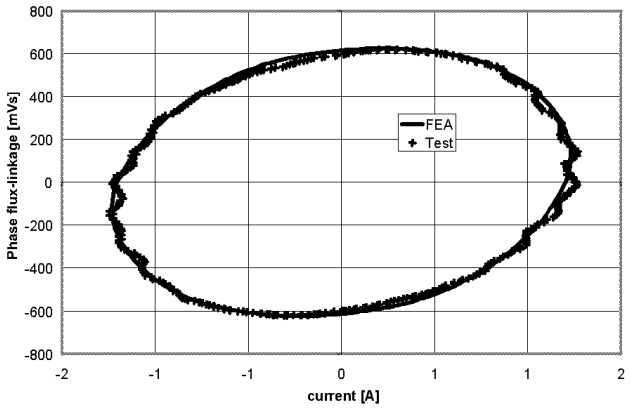

Figure 5. *i*-ψ loop for sinewave current control

Fig. 5 shows the *i*-ψ loop diagram for sinewave current control, comparing the measured loop with the finite-element calculation having a peak phase current of 1.23 A at 440 rpm with no phase advance. The loop torque is 1.10 Nm and this agrees almost exactly with the measured value. Both the current and the flux-linkage waveforms are closely sinusoidal in this condition.

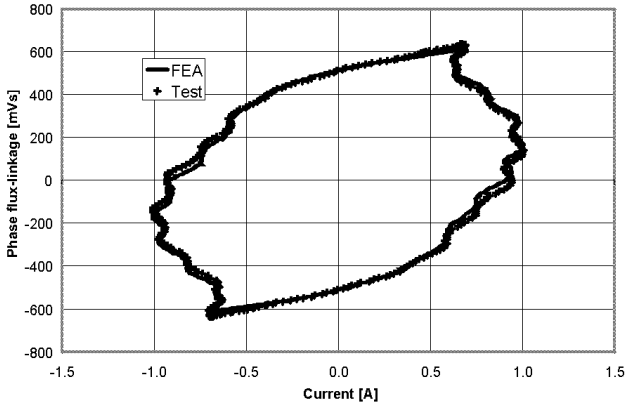

Figure 6. *i*-ψ loop for sinusoidal voltage-PWM control

Fig. 6 shows a sinusoidal voltage-PWM control in which the switching duty-cycle is modulated to give a sinusoidal terminal voltage (apart from the switching harmonics). Accordingly the flux-linkage is nearly sinusoidal but the current is not perfectly sinusoidal. The calculated loop in Fig. 6 is obtained by a current-driven finite-element computation using the measured current waveform, giving a loop torque of 0.79 Nm compared with the measured value of 0.76 Nm.

Fig. 7 shows the *i*-ψ loop for six-step operation at 528 rpm with a DC link voltage of 70 V. The calculated loop is obtained by a current-driven finite-element computation using the measured current waveform, giving a loop torque of 1.14 Nm compared with the measured value of 1.17 Nm. The current for this six-step condition is shown in Fig. 8, and the flux-linkage in Fig. 9. The flux-linkage waveform consists essentially of straight-line segments while the phase voltage waveform can be reconstructed by differentiating this waveform and adding the resistive volt-drop, as shown in Fig. 10.

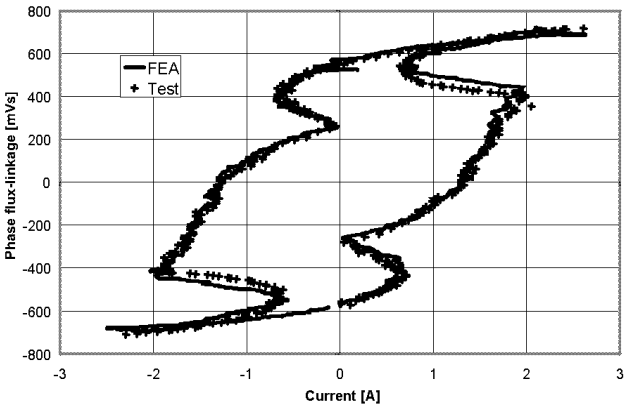

Figure 7. *i*-ψ loop for six-step operation

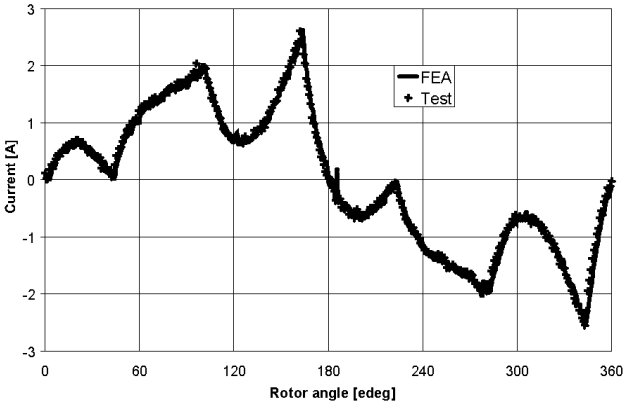

Figure 8. Current in six-step operation

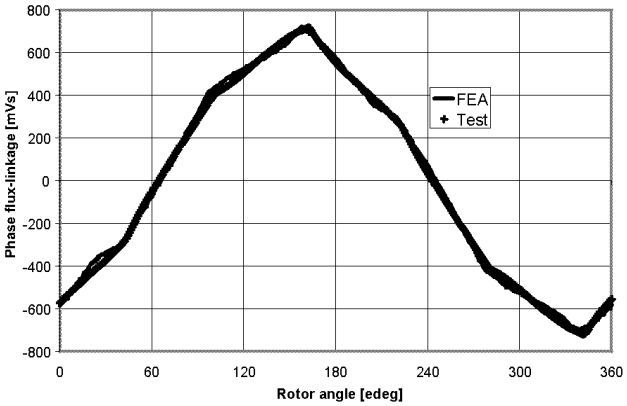

Figure 9. Phase flux-linkage in six-step operation

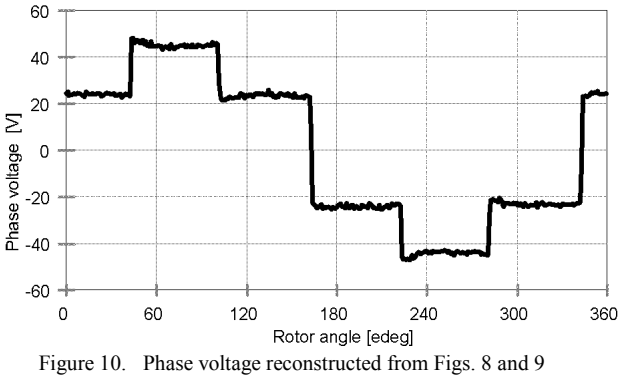

Figure 10. Phase voltage reconstructed from Figs. 8 and 9

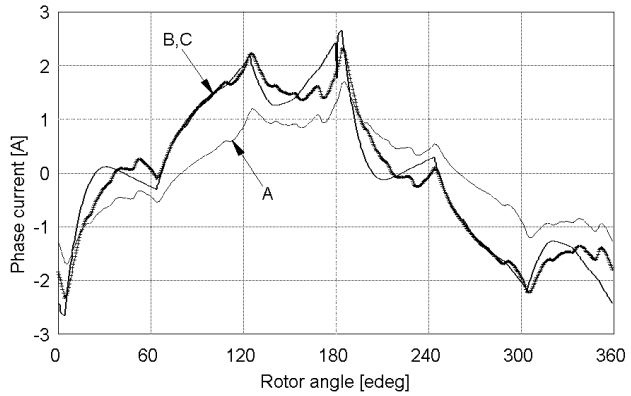

Figure 11. Computed current for six-step operation

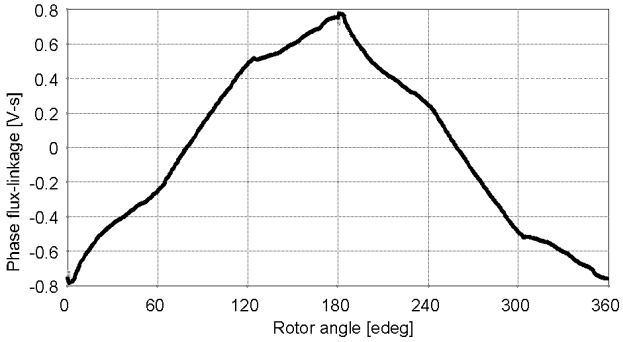

Figure 12. Computed flux-linkage for six-step operation

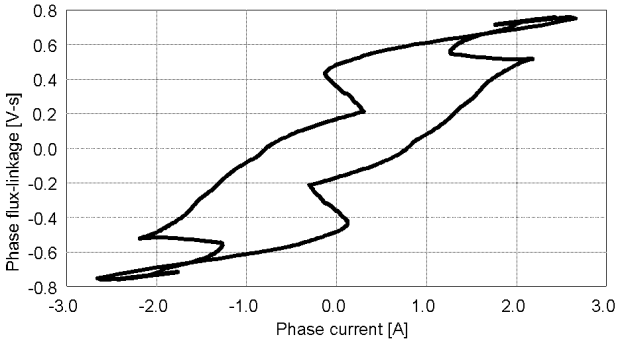

Figure 13. Computed *i*-ψ loop for six-step operation

V. Computation of the Six-Step Operating Point

To illustrate the effectiveness of the computation methods A, B and C of Section III above, the six-step drive is taken as the clearest example of a case where the applied voltage waveform is known *a priori*, but the current waveform is not.

Considering method C first, Figs. 11, 12 and 13 are computed from scratch using motor dimensions and materials, with the time-stepping solution of the differential circuit equations in the *PC-BDC* program and the values of L_d, L_q and Ψ_M updated by a finite-element calculation at each time-step using [11]. The electromagnetic torque computed from the loop area in Fig. 13 is 1.07 Nm compared with the measured value 1.17 Nm and the earlier finite-element calculation (current-driven with the measured current waveform) of 1.14 Nm. The solution takes about 1 hour on an 800 MHz laptop computer.

Also shown (dotted) in Fig. 11 is the current computed by method B with *fixed* values of L_d, L_q and Ψ_M after adjusting to match a current-driven finite-element loop calculation at 2.5A peak. The adjustments required a 15% reduction in *d*-axis magnet flux Ψ_M, a 40% reduction in X_d, and a 72% reduction in X_q to allow for the very strong saturation at this condition. The loop torque compares closely with that of method D.

Fig. 11 also shows the current computed by method A with fixed *unsaturated* inductances L_d and L_q and magnet flux-linkage Ψ_M (eqn. (7)). The current is underestimated and so is the torque, even though the flux-linkage waveform is the same.

VI. Conclusion

A computationally efficient method for incorporating finite-element solutions into a "voltage-driven" simulation of a brushless interior PM motor has been described. The flux-MMF diagram is used to compute the average torque, and results are compared with test measurements on a small machine.

Acknowledgment

We would like to thank P. Scavenius, N.-C. Weihrauch, and P. Hansen of Danfoss Compressors, Flensburg, Germany, who supplied the special test motor used in this paper. We would also like to acknowledge the support of the member companies of the *SPEED* Consortium and the assistance of P. Miller and I. Young of the *SPEED* Laboratory.

References

1. Boldea I., Tutelea L and Ilie Pitic C, *PM-Assisted Reluctance Synchronous Motor/Generator (PM-RSM) for Mild Hybrid Vehicles: Electromagnetic Design*, IEEE Trans. Ind. Appl., vol. 40, March/April 2004, pp. 492-498
2. Štumberger B, Štumberger G, Dolinar D, Hamler A and Trlep M, *Evaluation of Saturation and Cross-Magnetization Effects in Interior Permanent-Magnet Synchronous Motor*, IEEE Trans. Ind.Appl., Vol. 39, No. 5, September/October 2003, pp. 1264-1271
3. Bianchi N and Bolognani S, *Magnetic Models of Saturated interior Permanent Magnet Motors based on Finite Element Analysis*, IEEE Ind. Appl. Soc. Ann. Mtg., Conference Record, St. Louis, 1998, pp. 27-34
4. Bianchi N and Bolognani S, *Saturation effect on parameters and volt-ampere ratings of an interior PM motor for a spindle drive*, Proc. Electrical Drives Design and Applications, EPE'99, Lausanne, Switzerland, 1999
5. Jahns TM, Kliman GB and Neumann TW: *Interior permanent-magnet synchronous motors for adjustable-speed drives*, IEEE Trans. Ind. Appl., Vol. 22, 1986, pp. 738-747
6. Miller TJE : *Methods for testing permanent-magnet AC motors*. IEEE Ind. Appl. Soc. Ann. Mtg. (IAS), Toronto, October 1981, pp.494-499.
7. Staton DA, Soong, WL, Deodhar RP and Miller TJE: *Torque prediction using the flux-MMF diagram in AC, DC and reluctance motors*, IEEE Trans. Ind. Appl., Vol.32, No.1, Jan-Feb. 1996, pp.180-188.
8. Jabbar MA, Zhejie L, and Jing D: *Time-stepping finite-element analysis for the dynamic performance of a permanent magnet synchronous motor,* IEEE Trans. Magnetics, Vol. 39, No. 5, September 2003, pp. 2621-2623
9. Fitzgerald AE and Kingsley C Jr, *Electric Machinery*, McGraw-Hill, Second Edition 1961, New York
10. Hendershot JR and Miller TJE, *Design of brushless permanent-magnet motors*, ISBN 1-881855-03-1, www.motorsoft.com
11. Miller TJE, *PC-BDC* and *PC-FEA* Manuals, SPEED Laboratory, 2004.
12. Miller TJE, *SPEED's Electric Motors*, ISBN 1-881855-10-4, www.speedlab.co.uk